NANO LETTERS

Letter

pubs.acs.org/NanoLett

Direct Measurement of Band Edge Discontinuity in Individual Core–Shell Nanowires by Photocurrent Spectroscopy

Guannan Chen,[†] Guan Sun,[‡] Yujie J. Ding,[‡] Paola Prete,[§] Ilio Miccoli,[∥] Nico Lovergine,[∥] Hadas Shtrikman,[⊥] Patrick Kung,[¶] Tsachi Livneh,[#] and Jonathan E. Spanier*[,†]

[†]Department of Materials Science and Engineering, Drexel University, Philadelphia, Pennsylvania, United States

[‡]Department of Electrical and Computer Engineering, Lehigh University, Bethlehem, Pennsylvania, United States

[§]Istituto per la Microelettronica e Microsistemi (IMM), Consiglio Nazionale delle Ricerche (CNR), Lecce, Italy

[∥]Department of Innovation Engineering, University of Salento, Lecce, Italy

[⊥]Braun Center for Submicron Research, Condensed Matter Physics Dept., Weizmann Institute of Science, Rehovot 76100, Israel

[¶]Department of Electrical and Computer Engineering, University of Alabama, Tuscaloosa, Alabama, United States

[#]Department of Physics, Nuclear Research Center, Negev, P.O. Box 9001, Beer-Sheva 84190, Israel

Supporting Information

ABSTRACT: Group III–V coaxial core–shell semiconducting nanowire heterostructures possess unique advantages over their planar counterparts in logic, photovoltaic, and light-emitting devices. Dimensional confinement of electronic carriers and interface complexity in nanowires are known to produce local electronic potential landscapes along the radial direction that deviate from those along the normal to planar heterojunction interfaces. However, understanding of selected electronic and optoelectronic carrier transport properties and device characteristics remains lacking without a direct measurement of band alignment in individual nanowires. Here, we report on, in the GaAs/$Al_xGa_{1-x}As$ and GaAs/AlAs core–shell nanowire systems, how photocurrent and photoluminescence spectroscopies can be used together to construct a band diagram of an individual heterostructure nanowire with high spectral resolution, enabling quantification of conduction band offsets.

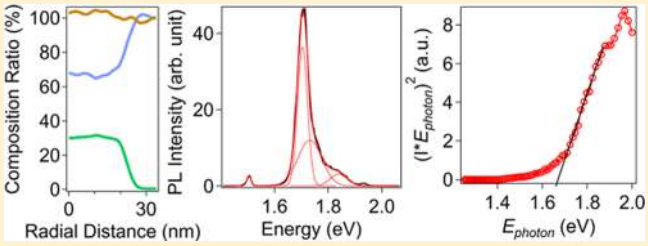

KEYWORDS: *photocurrent spectroscopy, core-shell nanowires, band offset*

Group III–V core–shell nanowires attract interest as integral materials in high performance electronic devices, even surpassing state-of-the-art Si transistors,[1] enabling signal phase modulation with hot electron transfer,[2] solving persistent challenges of silicon integration and elusive green wavelength emission in light-emitting devices.[3,4] To advance, however, from a concept-proving to a product-manufacture level, more-precise control in growth, accurate monitoring of doping level and carrier concentration, and knowledge of the nature of the interface of core–shell heterostructure and its effect on devices fabricated are needed. Following intense study of growth mechanisms and efforts to control crystallographic phases,[5−7] significant progress in growing single-phase nanowires of exceptionally high crystalline quality has been made. In using the Hall effect adapted for nanowires, carrier concentration with high axial spatial resolution can be measured.[8] The coaxial interface of core–shell nanowires typically plays the central role in device design and functionality. For instance, in electron-transfer devices the band edge discontinuity ΔE_C directly determines the transfer threshold and bias-dependent rate. Monitoring the interface within single nanowire, however, remains challenging. In planar heterojunctions, optical methods are frequently used to measure band edge offsets. For instance, X-ray photoemission spectroscopy (XPS) can be used to measure the valence band offset by quantifying the binding energy difference, enabling construction of a band diagram based on the valence band difference.[9] An additional limit of using XPS for band offsets in nanowires is that the signal from a single nanowire is too weak to detect, requiring ensemble characterization.

An additional complication that limits the prediction of band structure in core–shell nanowires involves the growth process. A large proportion of reported works in nanowires device prototyping use metal–organic vapor phase epitaxy (MOVPE) in nanowire synthesis. However, the shell growth in MOVPE core–shell nanowires usually involves a high-temperature process to suppress the metal-catalyzed growth of the core, which is known to add the uncertainty of the uniformity of shell composition.[10] Photoluminescence (PL) is widely used as initial characterization of the growth quality, doping, and defect

Received: May 12, 2013
Revised: July 22, 2013
Published: August 12, 2013

   dx.doi.org/10.1021/nl401737u | *Nano Lett.* 2013, 13, 4152–4157

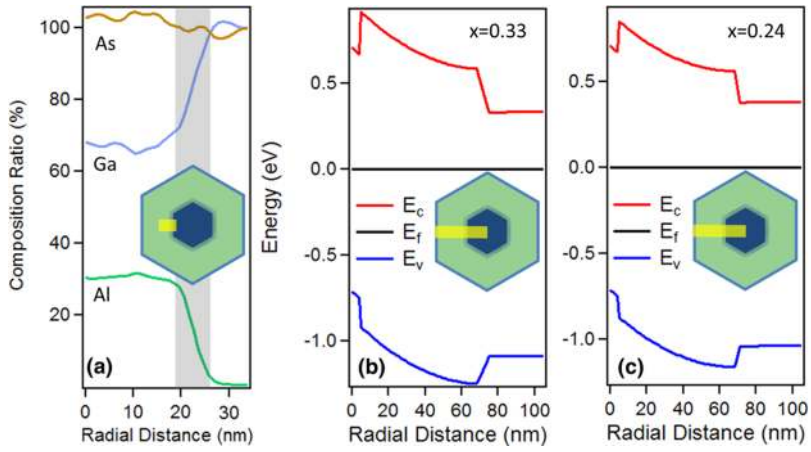

Figure 1. (a) Radial composition profile near the core−shell interface (x = 0.33), obtained from atom-probe tomography (APT, Supporting Information). The dark-shaded area in the illustration denotes the interface transition region. (b,c) Radial band diagram of a core−shell nanowire obtained via a 1D numerical Poisson-Schrödinger solver. The yellow stroke lines indicate the spatial line width of the APT data and simulations on the nanowire.

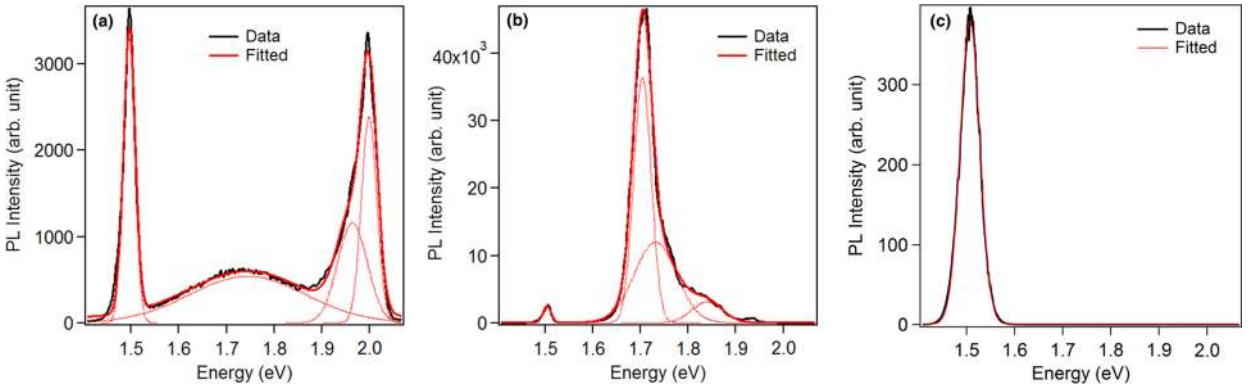

Figure 2. Low-temperature PL at 8.7 K from ensembles of (a) GaAs/$Al_{0.33}Ga_{0.67}As$ nanowires, (b) GaAs/$Al_{0.24}Ga_{0.76}As$ nanowires, and (c) GaAs/AlAs nanowires dispersed on SiO_2/Si substrate. Data are plotted in black; the red dotted lines show that the lineshapes are well-described by Gaussian fitting.

conditions in nanowires, and heterogeneous broadening of the PL lineshapes is expected for ensemble measurements. However, using PL as an effective method to characterize band edge discontinuity on single nanowire device is experimentally challenging due to requirements including focusing, precise positioning, and stability against drift. PL collection is also usually at a temperature much lower than normal device operation temperature for high spectral resolution. A direct electrical characterization of band alignment in nanowire devices intended for room temperature operation is sought but thus far lacking. Here we report on how photocurrent spectroscopy and analysis in conjunction with variable-temperature ensemble PL characterization enables facile measurement of the band edge offset from an interfacial optical transition within a coaxial core−shell nanowire, using the MOVPE-grown GaAs/$Al_xGa_{1-x}As$ ($x < 0.4$) as an example of a direct bandgap material and GaAs/AlAs nanowires grown by molecular beam epitaxy (MBE) as indirect one.

GaAs/$Al_xGa_{1-x}As$ nanowires with a core diameter of 60 nm, a shell thickness of 70 nm and a GaAs capping layer ∼5 nm (x = 0.24 and x = 0.33) used in this study are grown by Au-nanoparticle-catalyzed MOVPE method on 111(B)-terminated GaAs substrates as previously reported.[11] The GaAs/AlAs nanowires with a 100 nm GaAs core, a thinner AlAs shell of 10 nm and a thin GaAs cap (∼10 nm) to protect the shell are grown by MBE using a self-catalyzed method on Si(111) substrate (see Supporting Information). Both types of nanowires are in zinc-blende (ZB) phase. In GaAs/AlGaAs nanowires, the core is lightly p-typed unintentionally doped.[2] On the other hand, the shell is n-doped due to Si contamination from the Al precursor. Atom probe tomography (APT) results reveal a nearly linear-graded heterojunction of 6.5 nm at the interface of a GaAs/$Al_{0.33}Ga_{0.67}As$ nanowire (Figure 1a),[12] at a rate of 5.5%/nm (see also Supporting Information). The APT results for GaAs/$Al_{0.24}Ga_{0.76}As$ nanowires indicate a steeper transition at a rate of 8.3%/nm, where the junction width is 2.9 nm. The composition variation away from the interface is minimal. The band diagram simulation from a self-consistent 1D Poisson-Schrödinger equations solver program is performed to identify the band bending condition at the interface (Figure 1b) with the incorporation of APT profiles.[13] The doping levels in GaAs and AlGaAs in the simulation are 10^{17} cm^{-3} and 10^{18} cm^{-3}, respectively. Two assumptions are made in these simulations: (1) midgap Fermi-level pinning on the surface; (2) the composition gradient is assumed to be linear. The junction widths from APT results are subject to broadening due to possible sidewall nanofacet geometries and Al-rich hexagonal corners.[14,15]

PL investigations on ensemble nanowires were performed to identify optical transitions and their energy levels. Nanowires

dx.doi.org/10.1021/nl401737u | *Nano Lett.* 2013, 13, 4152−4157

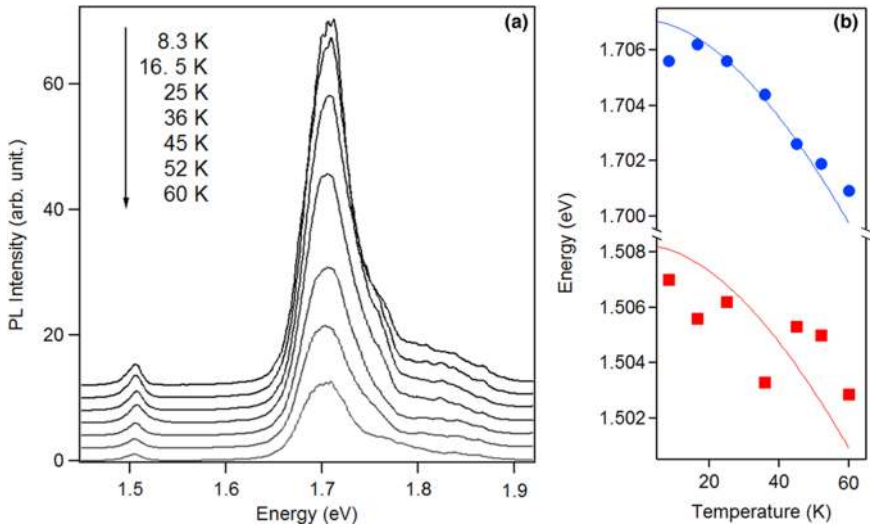

Figure 3. (a) Temperature-dependent PL from GaAs/$Al_{0.24}Ga_{0.76}As$ nanowires on SiO_2/Si substrate between 8.3 and 60 K. Spectra are offset for clarity. (b) Temperature-dependence of PL peak energy values of GaAs near bandgap transition (red squares) and interface transition (blue circles) from peak fittings. The solid lines show the fitting results of energy values using Varshni equation with offsets.

are transferred to a Si/SiO_2 substrate using a stamping process to eliminate luminescence from bulk GaAs substrate. A diode-pumped solid state (DPSS) 532 nm laser was used as excitation source for PL studies. The beam is focused on the sample with a spot size around 120 μm. The power range was between 1 and 100 mW by adjusting laser source current or using neutral density filters. Within this range no heating effect was observed. Low-temperature PL results collected at 8.7 K are shown in Figure 2. Three distinct peaks are seen in the spectrum of GaAs/$Al_{0.33}Ga_{0.67}As$ nanowires. The bandgap peaks are located at 1.505 and 1.976 eV for GaAs and $Al_{0.33}Ga_{0.67}As$, respectively. The shoulder on AlGaAs peak has an offset by 40 meV and originates from Si dopants with self-compensation.[16] The third peak at 1.723 eV corresponds to interface recombination, namely, electrons in the AlGaAs conduction band recombine with holes in the GaAs valence band. The intensity of interface transition peak is comparable to those of bandgap recombination which suggests that the overlap of electron and hole wave functions is large and confirms the direct nature of the transition.[17] The interface is more explicitly seen in the PL of GaAs/$Al_{0.24}Ga_{0.76}As$ nanowires with a peak appearing at 1.705 eV. The intensity of the peak exceeds the GaAs bandgap peak. The peak is partly convoluted with the AlGaAs peak (at 1.840 eV), the two being more closely spaced due to lower Al composition. The peak width at 8.7 K is on the order of 50 meV, only twice that of GaAs bandgap peak. In fact, the difference can be expected from the interface conditions discussed earlier. The narrower line width comes from the steeper transition at the interface on $x = 0.24$ nanowires, where the transition has a narrower distribution of energy on a junction width less than half of that in $x = 0.33$ nanowires. As a direct comparison, low-temperature (8 K) PL collected from a separate set of GaAs/$Al_{0.42}Ga_{0.58}As$ nanowires with indirect band gap shells grown by MOVPE showed only the broad impurity-dominant luminescence of low intensity (Supporting Information Figure S3). The indirect band gap shell requires phonon for transitions with the GaAs core, which eliminates the possibility of a direct optical transition.

A summary of Gaussian-fitted peak, temperature-dependent PL energies measured in $x = 0.24$ nanowires under 4 mW of excitation power reveals that the interface and GaAs peaks are correlated in the redshift when temperature increases (Figure 3). Since the conduction band offset should be nearly temperature independent, we applied Varshni fittings with offset on both of the transitions using bulk GaAs parameters. The results showed good agreement of temperature dependence between two transitions, which further confirmed the interface transition nature of the 1.705 eV peak. The shoulder on the high energy side of this peak is possibly from Si deep level impurity, having temperature-dependent variation in intensity at a slower rate than that for band-to-band GaAs radiative recombination. The band edge peak persists even at room temperature while the AlGaAs peak is quenched above 120 K due to the activation of nonradiative recombination. The assignment of interface peak energies in $x = 0.24$ nanowires is more accurate than that for $x = 0.33$ nanowires. Although the interface transition energy is close to the theoretical value of bandgap energy of GaAs (1.519 eV) plus the conduction band offset energy (0.261 eV),[18] a precise value of the energy associated with the peak is difficult to assign due to heterogeneous broadening, in which the band edge alignment varies within the ensemble, and the involvement of competing broad, multiple-energy-level impurity luminescence, which is more sensitive to fluctuation than that from the total impurity concentration. Nevertheless, the interface transition provides a guideline for probing the band edge discontinuity using photocurrent spectroscopy.

Photocurrent spectroscopy has been proven a versatile method in probing bandgap, resonant optical modes,[19,20] and polarization anisotropy[21] within individual nanowires. It involves a combination of two physical processes, absorption and transport, both of which are subject to both the materials and the interface. Single-nanowire devices were prepared by e-beam lithography. To eliminate the additional complexity from the thermionic emission from the contact-nanowire energy barrier, an optimized contact method with functional metal layer consisting of Pd and Zn is applied to devices in this study to reduce the additional contact Schottky barrier heights which impede the photocurrent.[22] The contact resistance is lowered by 2 orders of magnitude compared to Ti/Au contacts after an

dx.doi.org/10.1021/nl401737u | *Nano Lett.* 2013, 13, 4152–4157

optimized rapid thermal annealing. The inset of Figure 4a shows a representative device geometry with a 2 μm contact separation and 1 μm contact width. Devices before and after annealing both showed high light response under illumination from a 150 W broad band halogen lamp and alternately, a CW Ti:Sapphire laser at 800 nm (M2, Glasgow, U.K.). The photocurrent spectroscopy measurements were performed using this Ti:S laser (tunable from 690 to 900 nm) and a pulsed supercontinuum source (NKT Compact, Denmark, tunable from 460 to 1000 nm) at room temperature.

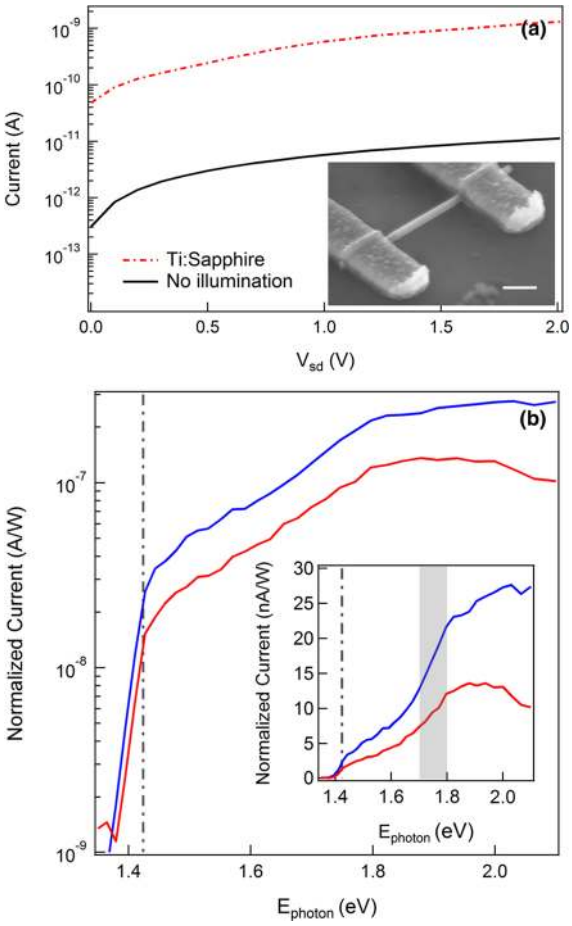

Figure 4. $I-V$ curves under laser illumination and dark conditions from a single GaAs/$Al_{0.33}Ga_{0.67}As$ nanowire device plotted on semilog scale. Inset: SEM image of a representative device (tilted at 52°; scale bar, 500 nm). (b) Normalized photocurrent spectra by incident photon flux in semilogarithm from two $x = 0.33$ representative devices. The inset shows the same plot on a linear scale to more clearly convey the increase of current around 1.7 eV.

We first discuss the results from GaAs/AlGaAs nanowires. We normalized the photocurrent by photon flux, that is, power per incident photon energy, to eliminate the spectral power variation, and the normalized photocurrent is proportional to optical absorption. Distinct absorption edges of GaAs core can be observed (Figure 4b), and at 300 K, the absorption edge is observed at 1.408 eV (881 nm), consistent with that from zinc-blende structures in nanowires possessing different shell Al compositions. Significantly, an additional steep rise of photocurrent with photon energy is seen near 1.675 eV (740 nm), at a value close to the interface transition observed in PL, indicating an enhancement in carrier photogeneration correlating with absorption of incident photons at the interface. At photon energy greater than AlGaAs bandgap, the photocurrent reaches a plateau due to the photogenerated electrons filling up the AlGaAs conduction band, competing with the transition from GaAs.

Since our photocurrent spectroscopy involves individual nanowires, the aforementioned issues relating to ensemble averaging in PL broadening are eliminated. Normalized photocurrent spectra are replotted as square of the product of normalized photocurrent (denoted as I^*) and photon energy, which is proportional to incident photon energy in a direct band gap transition. Similar approach but for indirect band gap transition (i.e., square root of I*) is also discussed below for GaAs/AlAs nanowires. Linear fitting on the conspicuous slope intersects the energy axis at the transition energy, that is, $\Delta E_C + E_{g,GaAs}$. The $x = 0.33$ nanowire device is seen to possess an intercept of 1.670 eV at 300 K (Figure 5a). With the GaAs core bandgap results a priori (1.408 eV), a ΔE_C (262 $\pm$ 40 meV) is unveiled in a single nanowire. While the method is comparable to the internal photoemission, which is also a photocurrent-based method used in planar devices,[23] the bias dependent band bending at the contact in internal

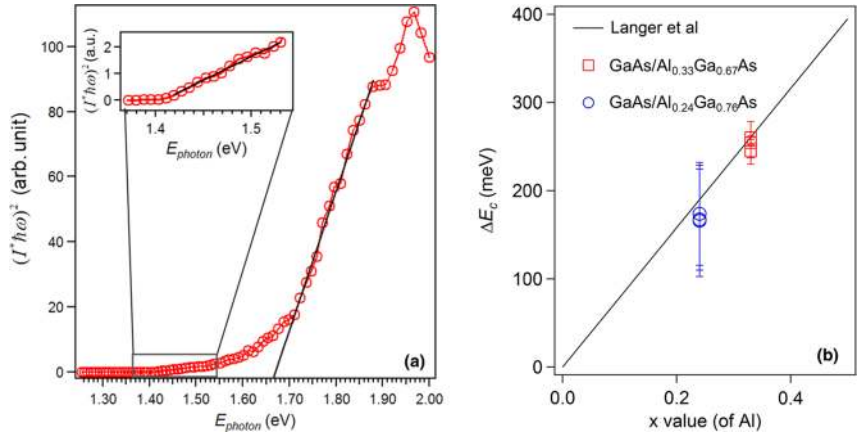

Figure 5. (a) Transformed photocurrent spectrum of one x = 0.33 nanowire device: the vertical coordinate is transformed to the square of normalized photocurrent and photon energy product. The solid lines are the linear fittings of curve slopes. Inset: an expanded view of the lower photon-energy range portion and slope corresponding to the GaAs bandgap energy. (b) Conduction band edge offsets for different Al composition shell. The background solid line is an empirical linear dependence reproduced from Langer et al.[24]

dx.doi.org/10.1021/nl401737u | *Nano Lett.* 2013, 13, 4152–4157

photoemission requires an additional extrapolation for flat band voltage rather than direct measurement. In our case, band bending is alleviated by the ohmic contact scheme and does not affect the threshold energy of band edge transition, confirmed by the bias-independent intercept in the measured photocurrent spectra. The results are compelling through comparison of the ΔE_C values in nanowires with two different Al compositions (x = 0.24 and 0.33). We found good agreements between the spectrally derived ΔE_C with the Al composition dependent band offsets (Figure 5b).[24] Besides the resolution, photocurrent spectroscopy offers two additional advantages over the PL method, less constraint on temperature measurement and broader material compatibility in indirect gap materials. A strong near-bandgap peak of GaAs was observed at a wide range of temperature in GaAs/AlAs nanowires that usually have a low impurity level. However, neither interface or AlAs luminescence was observed in temperature-dependent PL since AlAs is an indirect bandgap material and there is no Si impurity present (Figure 2c and Figure S1). In contrast and significantly, we found in MBE-grown GaAs/AlAs core−shell nanowires that photocurrent spectroscopy also reveals the band edge alignment when the spectra are transformed into the square root of normalized photocurrent, corresponding to an indirect transition since AlAs is an indirect bandgap semiconductor (Figure 6). The extrapolated conduction band offset

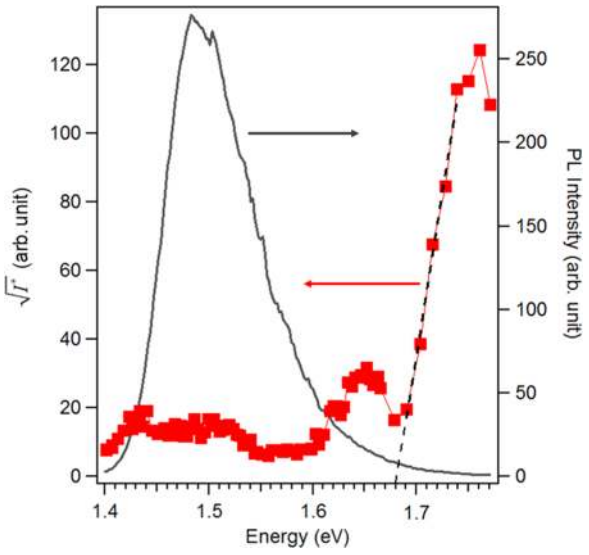

Figure 6. Photocurrent spectrum from a GaAs/AlAs nanowire transformed to square-root of normalized photocurrent (red) and room-temperature photoluminescence (gray). The black dotted line is the linear fitting of the curve slope.

(0.274 eV) is also close to the planar value (0.283 eV).[25] The result is therefore promising for extending this method to core−shell nanowires with one or both consisting of indirect bandgap materials.

In summary, photocurrent spectroscopy and analysis, coupled with results from ensemble PL and supported by simulation as presented here represent a facile means of obtaining the band-edge discontinuity within individual coaxial core−shell semiconductor nanowire heterojunctions without the complications presented by ensemble averaging. In addition to enabling quantification of the wire-to-wire variation in conduction band offsets, we anticipate that the quantifying enabled by this approach will permit more informed study, design, and device application of the spatial and temporal trajectory of hot photoexcited carriers at and near nanowire heterojunction interfaces.

■ ASSOCIATED CONTENT

Supporting Information

Additional information and figures. This material is available free of charge via the Internet at http://pubs.acs.org.

■ AUTHOR INFORMATION

Corresponding Author

*E-mail: spanier@drexel.edu.

Notes

The authors declare no competing financial interest.

■ ACKNOWLEDGMENTS

The authors thank Zongquan Gu and Kevin Siegl for assistance with implementing Poisson-Schrödinger simulations. Work at Drexel University is supported by NSF (DMR 0907381), and G.C. and J.E.S. acknowledge partial support from the ARO (W911NF-08-1-0067 and a DURIP instrumentation award for the acquisition of laser sources used in this work). P.P., I.M., and N.L. acknowledge Fabio Marzo for assisting with the experimental growth work. H.S. acknowledges partial support from the Israel Science Foundation (Grant 532/12 ISF) and from the Israeli Ministry of Science and Technology (Grant 3-6799 IMOST). P.K. acknowledges partial support from NSF (DMR-0907558).

■ REFERENCES

(1) Tomioka, K.; Yoshimura, M.; Fukui, T. *Nature* **2012**, *488*, 189−192.
(2) Chen, G.; Gallo, E. M.; Leaffer, O. D.; McGuckin, T.; Prete, P.; Lovergine, N.; Spanier, J. E. *Phys. Rev. Lett.* **2011**, *107*, 156802.
(3) Qian, F.; Gradecak, S.; Li, Y.; Wen, C.-Y.; Lieber, C. M. *Nano Lett.* **2005**, *5*, 2287−2291.
(4) Tomioka, K.; Motohisa, J.; Hara, S.; Hiruma, K.; Fukui, T. *Nano Lett.* **2010**, *10*, 1639−1644.
(5) Krogstrup, P.; Popovitz-Biro, R.; Johnson, E.; Madsen, M. H.; Nygård, J.; Shtrikman, H. *Nano Lett.* **2010**, *10*, 4475−82.
(6) Joyce, H. J.; Wong-Leung, J.; Gao, Q.; Tan, H. H.; Jagadish, C. *Nano Lett.* **2010**, *10*, 908−915.
(7) Lehmann, S.; Jacobsson, D.; Deppert, K.; Dick, K. A. *Nano Res.* **2012**, *5*, 470−476.
(8) Storm, K.; Halvardsson, F.; Heurlin, M.; Lindgren, D.; Gustafsson, A.; Wu, P. M.; Monemar, B.; Samuelson, L. *Nature Nanotechnol.* **2012**, *7*, 718−722.
(9) Kraut, E.; Grant, R.; Waldrop, J.; Kowalczyk, S. *Phys. Rev. Lett.* **1980**, *44*, 1620−1623.
(10) Jiang, N.; Parkinson, P.; Gao, Q.; Breuer, S.; Tan, H. H.; Wong-Leung, J.; Jagadish, C. *Appl. Phys. Lett.* **2012**, *101*, 023111.
(11) Prete, P.; Marzo, F.; Paiano, P.; Lovergine, N.; Salviati, G.; Lazzarini, L.; Sekiguchi, T. *J. Cryst. Growth* **2008**, *310*, 5114−5118.
(12) Dawahre, N.; Shen, G.; Balci, S.; Baughman, W.; Wilbert, D. S.; Harris, N.; Butler, L.; Martens, R.; Kim, S. M.; Kung, P. *J. Electron. Mater.* **2011**, *41*, 801−808.
(13) Tan, I.-H.; Snider, G. L.; Chang, L. D.; Hu, E. L. *J. Appl. Phys.* **1990**, *68*, 4071−4076.
(14) Wolf, D.; Lichte, H.; Pozzi, G.; Prete, P.; Lovergine, N. *Appl. Phys. Lett.* **2011**, *98*, 264103.
(15) Rudolph, D.; Funk, S.; Döblinger, M.; Morkötter, S.; Hertenberger, S.; Schweickert, L.; Becker, J.; Matich, S.; Bichler, M.; Spirkoska, D.; Zardo, I.; Finley, J.; Abstreiter, G.; Koblmueller, G. *Nano Lett.* **2013**, *13*, 130321124359003.

(16) Oelgart, G.; Lippold, G.; Proctor, M.; Martin, D.; Reinhart, F. K. *Semicond. Sci. Technol.* **1991**, *6*, 1120−1125.
(17) Arif, R. A.; Zhao, H.; Tansu, N. *Appl. Phys. Lett.* **2008**, *92*, 011104.
(18) Adachi, S. *J. Appl. Phys.* **1985**, *58*, R1−R29.
(19) Cao, L.; Nabet, B.; Spanier, J. E. *Phys. Rev. Lett.* **2006**, *96*, 157402.
(20) Cao, L.; White, J. S.; Park, J.-S.; Schuller, J. A.; Clemens, B. M.; Brongersma, M. L. *Nat. Mater.* **2009**, *8*, 643−647.
(21) Persano, A.; Nabet, B.; Taurino, A.; Prete, P.; Lovergine, N.; Cola, A. *Appl. Phys. Lett.* **2011**, *98*, 153106.
(22) Bruce, R.; Clark, D.; Eicher, S. *J. Electron. Mater.* **1990**, *19*, 225−229.
(23) Abstreiter, G.; Prechtel, U.; Weimann, G.; Schlapp, W. *Physica B +C* **1985**, *134*, 433−438.
(24) Langer, J.; Heinrich, H. *Phys. Rev. Lett.* **1985**, *55*, 1414−1417.
(25) Massidda, S.; Min, B.; Freeman, A. *Phys. Rev. B* **1987**, *35*, 9871−9874.